II Rheometry

II.1 Introduction

Structured materials are generally composed of microstructures dispersed in a homogeneous phase [30]. These materials usually have a yield stress, i.e. a threshold stress beyond which the viscosity of the material thin dramatically. Viscoplastic or yield stress materials are found in a wide variety of industries such as food, cosmetic, farmaceutical and petroleum. In these industries, knowing the accurate rheological properties of a viscoplastic material is fundamental for the success of many operations. Nevertheless, the rheometry of structured materials still presents some challenges, such as yield stress measurements, apparent wall slip, thixotropy and the breakdown of structure on loading the material into the geometry used.

In experimental studies involving flows of viscoplastic materials through different geometries it is frequently necessary to use a yield-stress model material [31]. A good model for its purpose needs to be transparent, inexpensive, and relatively easy to prepare and to modify the rheological properties. Among many thickeners that can be found, Carbopol is one of the most popular due to its characteristics [23]. Carbopol gels behave like a viscoplastic material and can be considered a two-phase dispersion of swollen micro-gel particles in water [32].

One of the main problems in the rheometry of this kind of material is the presence of apparent wall slip during measurements. Barnes [33] performed a comprehensive review about the subject. Apparent slip, or wall depletion effects, can occur in flows of structured materials. It consists in a displacement of the disperse phase away from the solid boundaries, leaving a lower-viscosity, depleted layer of fluid adjacent to the wall. This lower-viscosity depleted layer turns easier any flow over the boundary due to lubrication effect. This phenomenon is observed mainly in flows of structured materials with low shear rates, large components as the disperse phase, smooth walls and small dimensions. In general, apparent wall slip occurs in such a way that the apparent viscosity measured with different size geometries is not equal, and lower viscosities are obtained with smaller geometries. In addition, an apparent yield stress at lower stresses and sudden breaks in the flow curve can also be seen [33, 34].

The apparent slip of structured materials can be characterized by giving enough data with different size geometries and then by doing a number of mathematical manipulations so as to end up with the bulk flow properties. On the other hand, as an attempt to eliminate wall slip during measurements and characterize the bulk material, several new rheometer geometries have been proposed by altering the physical or chemical character of the walls [33, 35].

A common artefact to avoid wall depletion effects is to rough the surface (this is used in plate-plate and bob-in-cup geometries), which breaks the depleted layer of fluid if this layer is very thin. Other alternative is the vane geometry, a central shaft with a small number of thin blades arranged around at equal angles. The vane geometry, exploited by Nguyen and Boger [36, 37] to measure the yield stress of concentrated suspensions has become a popular tool to characterize yield stress materials since then [38, 39, 40, 41]. The vane method consists in substituting the inner cylinder by the vane and in assuming that the stress is uniformly distributed on a cylindrical sheared surface around the blades to calculate the yield stress from the maximun torque [36, 37]. Another consideration often used is that the apparent slip occurs only at the inner cylinder. It is based on Buscall et al. [42] who found no slip at the outer cylinder for weakly attracted particle dispersions. However, Barnes proposed the addition of a slender gauze basket inserted inside an outer cylinder so as to eliminate apparent slip at the outer smooth wall, since wall depletion effects can be found in rheological measurements of other structured materials with simple vane geometry [43].

In this chapter, the traditional smooth Couette (bob-in-cup), the simple vane and a modified grooved Couette are analyzed experimentally and numerically so as to evaluate their performance in the rheometry of viscoplastic materials. The modified grooved Couette geometry consists in a bob-in-cup with vertical grooves both on the inner and on the outer cylinder. It follows the same idea of the vane and was employed to decrease the contact region between solid walls and the material along the sheared surface, avoiding the depletion phenomena. As a viscoplastic model material, aqueous Carbopol dispersions were used.

II.2 Analysis

(a) Experimental measurements

Although the concept of the use of two concentric cylinders for measuring the shear viscosity of different materials goes back to Stokes and Margules [44, 45], the development of this geometry for its purpose is attributed to Maurice Couette [46] since he was the first to control this apparatus [47]. The measurements of the rheological properties in rotational rheometers are done applying a torque or a rotation in one of the cylinders and measuring the resulting quantity at the same cylinder or at the other one. A scheme of the bob-in-cup geometry is shown in Fig. II.1. The following hypotheses are considered: (i) steady and laminar flow, (ii) axisymmetric flow, (iii) neglect end and gravity effects. Therefore, the flow is considered azimuthal ($v_\theta = \Omega r, v_r = v_z = 0$).

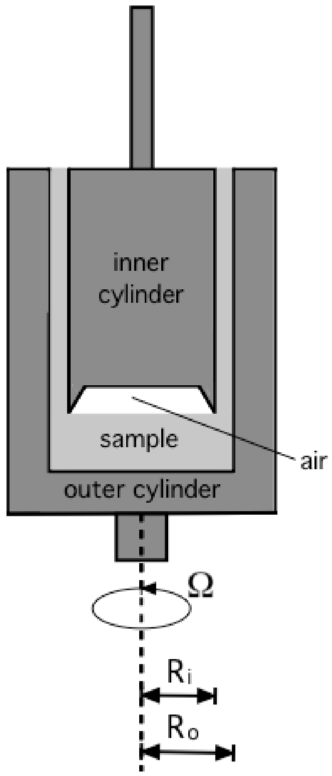

Figure II.1: Scheme of bob-in-cup geometry.

In the instrument used in the experiments, the rotational velocity Ω is applied in the outer cylinder, and the torque T is measured at the inner cylinder. Since 0.90> R_i/R_o >0.99, the wall shear stress is related to the torque T by:

$$\tau = \frac{T}{4\pi L}\left(\frac{R_i^2 + R_o^2}{R_i^2 R_o^2}\right) \tag{1}$$

where T is the torque at the inner cylinder wall and L is the inner cylinder length. The wall shear rate $\dot{\gamma}$ is related to the rotational velocity (for 0.90> R_i/R_o >0.99) by:

$$\dot{\gamma} = \left(\frac{R_i^2 + R_o^2}{R_o^2 - R_i^2}\right)\Omega \tag{2}$$

where Ω is the rotation velocity of the outer cylinder. Therefore, the viscosity is determined by:

$$\eta = \frac{\tau}{\dot{\gamma}} = \frac{T(R_i^2 + R_o^2)/(4\pi L R_i^2 R_o^2)}{\Omega(R_i^2 + R_o^2)/(R_o^2 - R_i^2)} \Rightarrow \eta = \frac{T}{\Omega 4\pi L}\left(\frac{R_o^2 - R_i^2}{R_i^2 R_o^2}\right) \tag{3}$$

The viscosity using the vane and grooved geometries is also determined by Eq. (3). In these cases, the hypothesis that the flow kinematics is similar to the one that occurs in the smooth Couette geometry is adopted, considering that the material between blades/grooves moves together with the solid surfaces.

(b) Viscosity function and rheological parameters

In order to describe the behavior of the Carbopol dispersion, the SMD viscosity function proposed by de Souza Mendes and Dutra [24] was used in the mathematical modelling:

$$\eta = \left(1 - \exp\left[-\frac{\eta_o \dot{\gamma}}{\tau_o}\right]\right)\left(\frac{\tau_o}{\dot{\gamma}} + K\dot{\gamma}^{n-1}\right) \tag{4}$$

in this equation, $\dot{\gamma}$ is the shear rate, and the parameters η_o, τ_o, K, and n, are respectively the low shear rate viscosity, the yield stress, the consistency index, and the behavior or power-law index [24].

Defining $\dot{\gamma}_0 = \tau_0/\eta_0$, and $\dot{\gamma}_1 = (\tau_0/K)^{1/n}$, and choosing τ_0 as characteristic stress, and $\dot{\gamma}_1$ as characteristic shear rate, then

$$\tau^* = \frac{\tau}{\tau_0}; \qquad \dot{\gamma}^* = \frac{\dot{\gamma}}{\dot{\gamma}_1} \tag{5}$$

With Eq. (5) the SMD viscosity function can be written in the dimensionless form [25]:

$$\eta^* = \frac{\tau^*}{\dot{\gamma}^*} = (1 - \exp\left[-(J+1)\dot{\gamma}^*\right])\left(\frac{1}{\dot{\gamma}^*} + \dot{\gamma}^{*n-1}\right) \tag{6}$$

where τ^* is the dimensionless shear stress, $\dot{\gamma}^*$ is the dimensionless shear rate, n is the behavior or power-law index, and J is the jump number given by the following expression:

$$J \equiv \frac{\dot{\gamma}_1 - \dot{\gamma}_o}{\dot{\gamma}_o} \tag{7}$$

(c) Governing equations and boundary conditions

The governing equations can be written in the dimensionless form considering the following dimensioless variables:

$$\boldsymbol{v}^* = \frac{\boldsymbol{v}}{\dot{\gamma}_1 R_o}; \quad \boldsymbol{T}^* = \frac{\boldsymbol{T}}{\tau_o}; \quad p^* = \frac{p}{\tau_o}; \quad \nabla^* = R_o \nabla \tag{8}$$

where R_o is the outer cylinder radius, $\boldsymbol{v}$ is the velocity field, $\boldsymbol{T}$ is the stress field, and p is the pressure field.

The viscoplastic material is assumed to be homogeneous and incompressible. In this analysis the flow is bi-dimensional, neglecting end and gravity effects. The flow is considered to be laminar, steady, and inertialess. Thus, the dimensionless conservation equation of mass is given by:

$$\nabla^* \cdot \boldsymbol{v}^* = 0 \tag{9}$$

And the dimensionless momentum conservation equation becomes:

$$\nabla^* \cdot \boldsymbol{T}^* = \mathbf{0} \tag{10}$$

In this analysis it is also assumed that the material behaves like the generalized Newtonian material model [6], given by:

$$\boldsymbol{T}^* = -p^*\mathbf{1} + \boldsymbol{\tau}^* = -p^*\mathbf{1} + \eta^*(\dot{\gamma}^*)\dot{\boldsymbol{\gamma}}^* \tag{11}$$

where $\boldsymbol{\tau}^*$ is the extra-stress tensor field, $\dot{\boldsymbol{\gamma}}^* = \nabla^*\boldsymbol{v}^* + (\nabla^*\boldsymbol{v}^*)^T$ is the rate-of-deformation tensor field, $\dot{\gamma}^* \equiv \sqrt{tr\ \dot{\boldsymbol{\gamma}}^{*2}/2}$ is a measure of its intensity, and $\eta^*(\dot{\gamma}^*)$ is given by Eq. (6).

In all three geometries analyzed, the smooth Couette, the simple vane and the grooved Couette, the flow is considered bi-dimensional and the no-slip boundary condition is defined at walls. The inner cylinder is stagnant, and the outer cylinder rotates with an angular velocity equal to Ω (at $r = R_o$). So, at the inner cylinder $v^* = 0$, and at the outer cylinder $v^* = \Omega/\dot{\gamma}_1$.

II.3 Experiments

Figure II.2: The geometries.

As a viscoplastic model material, Carbopol dispersions in water with different concentrations and pH=7 was used. The experimental investigation was done using an ARES rotational rheometer, and three different geometries, shown in Fig. II.2:

- the original smooth Couette geometry (two concentric cylinders with smooth walls);
- the simple vane geometry (one outer cylinder with smooth wall and one bladed cylinder);

– the grooved Couette geometry (two concentric cylinders with grooved walls).

The vane geometry is a six-blades geometry, and the vanes are 9.65 mm deep and 2 mm wide. In the grooved geometry, the grooves are 1 mm deep and 2 mm wide, and are roughly 2 mm spaced.

II.4 Numerical Solution

The governing conservation equations of mass and momentum were discretized using the finite volume technique. The commercial software FLUENT was used in the numerical simulations. Two different models were used to take into account the cylinder rotation. For the smooth Couette and vane geometries, the Single Rotating Reference Frame (SRF) model [48] was employed, and all the conservation equations, Eqs. (9) and (10), are solved at the entire computational domain. For the grooved geometry, the Multiple Rotating Reference Frame (MRF) model [48] was used. In this case, part of the domain is solved using the moving reference frame equations (Eqs. (1) and (2)), and part considering stationary reference frame (i.e. $\Omega = 0$). At the interface between the two zones, a local reference frame transformation is performed so that variables in one zone can be used to calculate fluxes at the boundary of the adjacent zone [48].

For performing the numerical simulations, Carbopol 0.17% SMD parameters were used. The three geometries defined in the simulations were exactly the ones used in the experiments (shown in Fig. II.2), except for the fact that in the numerical simulations, a bi-dimensional approach is used, neglecting end effects. The inner/outer diameters, as well as the meshes used are depicted in Table II.1. The number of cells was chosen considering similar meshes in the annular space between cylinders.

Table II.1: Geometries and meshes.

Geometries	Number of Cells	Inner/Outer Diameter (mm)
Smooth Couette	28800	32/34
Vane	56160	32/34
Grooved Couette	130320	32/34

II.5 Results and Discussion

(a) Experimental Results

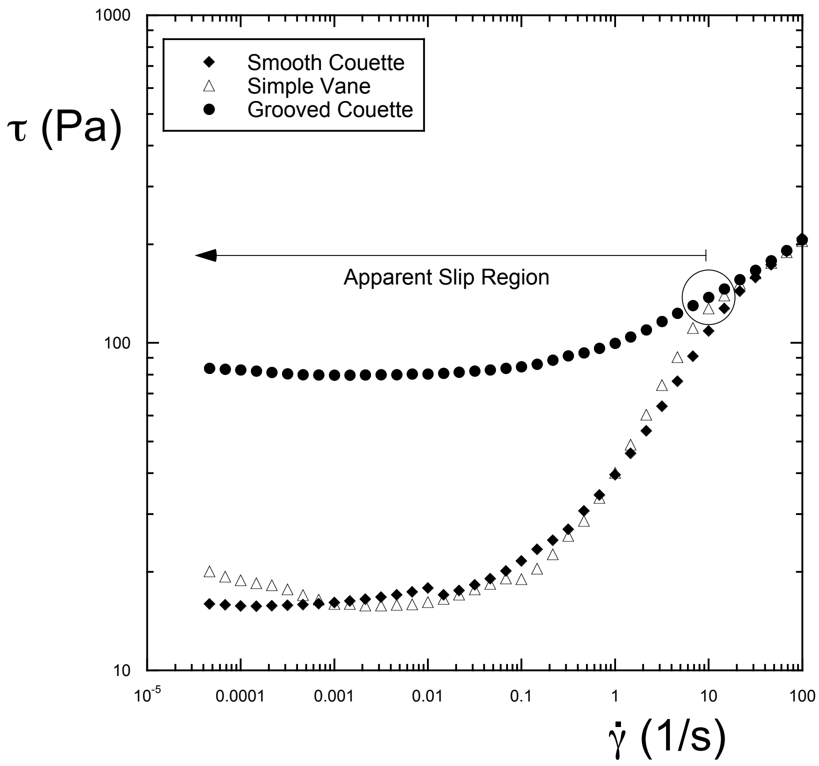

Figure II.3: Flow Curve of Carbopol dispersion 0,17% – investigation of the apparent slip region.

Figs. II.3 and II.4 show the flow curves obtained for the Carbopol dispersion 0.17%. Different results were obtained with the smooth Couette and vane geometries when compared to the grooved one. For low shear rates or stresses, the smooth Couette and vane geometries gave lower values of stresses, suggesting that apparent wall slip occurred for shear stresses lower than 105 Pa for this concentration of Carbopol. In these figures it is easy to observe an apparent slip region belong which the characterization of Carbopol dispersions becomes more complex. Moreover, it can be noted that once the vane is used to suppress the inner wall slip and the results obtained with the smooth Couette and vane were similar, apparent slip seems to occur mainly at the outer wall.

The Carbopol 0.17% yield stress was evaluated using the flow curve obtained with the grooved geometry shown in Fig. II.5, since it cannot be seen breaks in this flow curve, and consequently no apparent slip seems to occur. All rheological parameters for the SMD viscosity function — Eq. (4) — were obtained via curve fitting, also using the grooved geometry result.

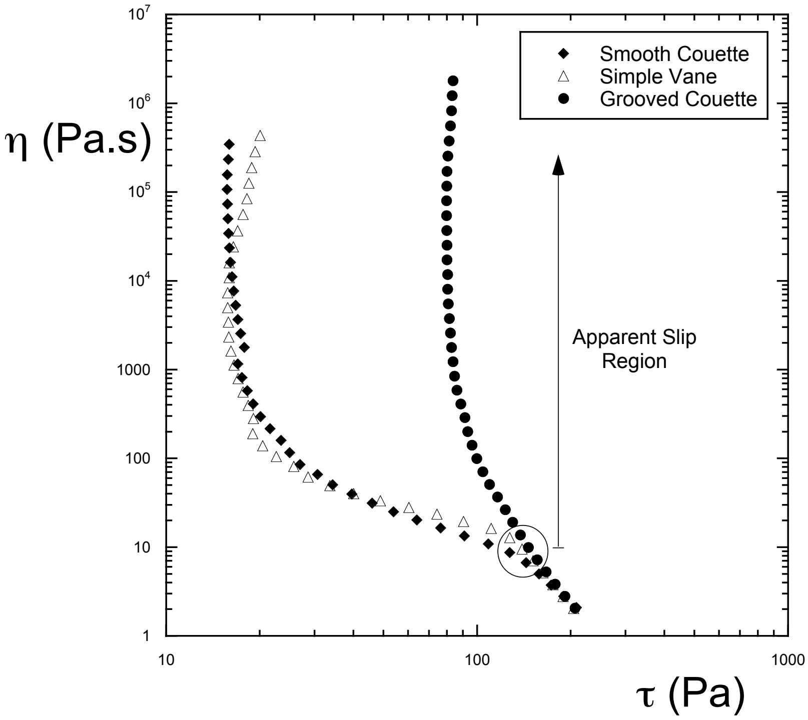

Figure II.4: Viscosity of Carbopol dispersion 0,17% as a function of shear stress – investigation of the apparent slip region.

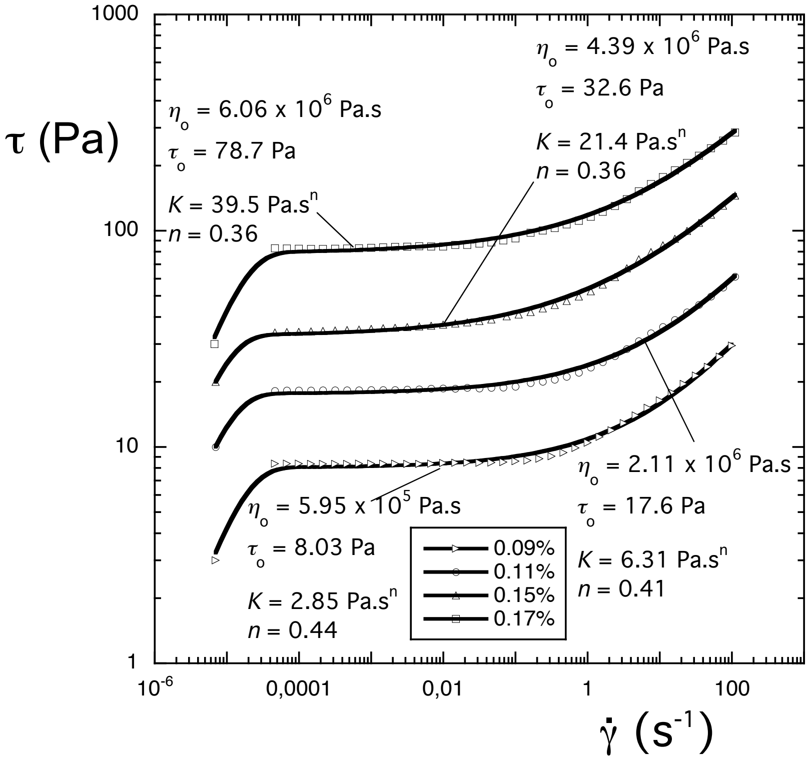

Figure II.5: Flow Curve of different Carbopol dispersions without apparent slip.

In Fig. II.5 is shown the flow curves for all concentrations of Carbopol investigated. All of these flow curves were obtained with the grooved Couette geometry so as to suppress the apparent slip in both walls (inner and outer). It is important to point out that in all of these flow curves, each data point was taken only after the steady state was achieved. The data-points corresponding to the lowest shear rate were obtained from creep experiments performed in a UDS 200 Paar-Phisica rheometer with a grooved Couette geometry (see Fig. II.7), since the rate-sweep tests of the ARES rheometer employed could not handle such low shear rates. In these creep tests, a constant stress below the yield stress was imposed, and, after a steady flow was reached, typically after up to 48 hours, the corresponding shear rate was obtained.

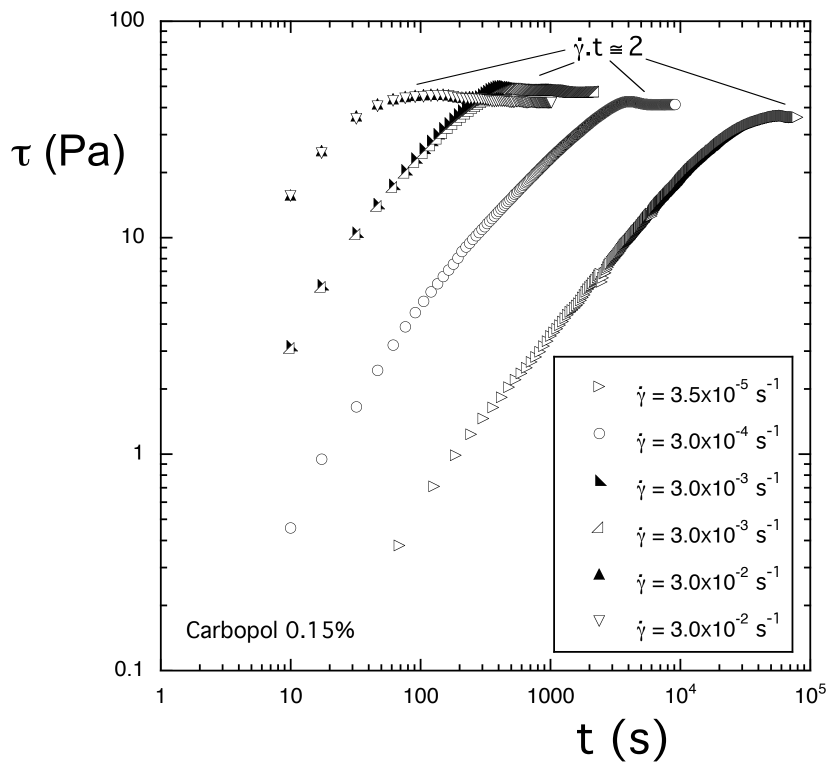

Figure II.6: Thixotropic Curves of Carbopol dispersion 0,15%.

Some thixotropic curves are shown in Fig. II.6 so as to illustrate the time needed to achieve the steady state for each shear rate in the flow curve. These curves were obtained by imposing a constant shear rate to a sample of Carbopol 0.15%. For each shear rate imposed, after waiting a specific time, the shear stress, and consequently the viscosity, achieved a constant value which corresponds to the steady data point plotted in the flow curve shown in Fig. II.5. By observing the thixotropic curves it can be seen that the specific time needed to achieve the steady flow increases in the same order of magnitude as the shear rate imposed decreases. Moreover, it is observed that the Hencky strain ($\dot{\gamma}.t$) is roughly equal to 2 for all shear rates. This evident fact leads to the conclusion that there is a minimum strain that needs to be attained so as to the steady flow be achieved. Similar curves were obtained for all concentrations of Carbopol investigated and similar results were observed. Although, only the curves of Carbopol 0.15% are shown in this thesis to illustrate this behavior due to space limitations.

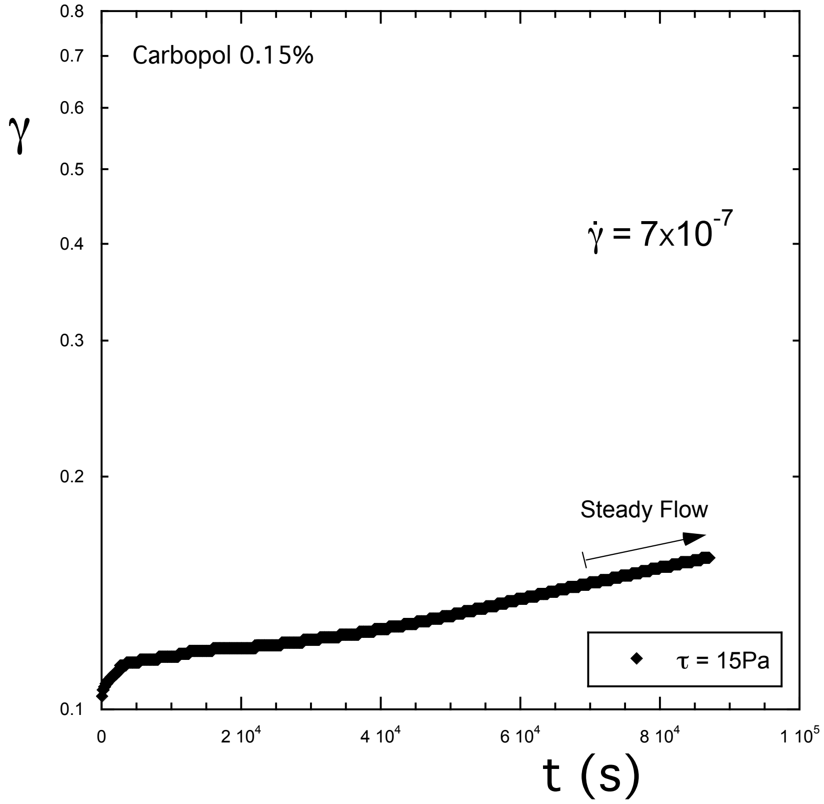

Figure II.7: Creep test realized in a UDS 200 Paar-Physica with a grooved Couette geometry of Carbopol dispersion 0,15%.

One example of creep test realized in a UDS 200 Paar-Physica is illustrated in Fig. II.7. As the thixotropic curves (Fig. II.6), this creep test was performed with Carbopol 0.15%. Basically, a constant shear stress lower than the yield stress was imposed to a sample of Carbopol 0.15% and the strain was measured as a function of time. After a specific time, the creep curve keep a fixed inclination which indicate that the steady flow was reached and the strain rate (which is equal to the shear rate in this case) becomes constant. In this example of creep test, a shear stress of 15 Pa was imposed to a Carbopol 0.15% and a shear rate of $7{\times}10^{-7}\,\mathrm{s}^{-1}$ was obtained, which corresponds to a steady data point in the flow curve of Carbopol 0.15%. All of the data-points corresponding to the lowest shear rate in the flow curves shown in Fig. II.5 were obtained with similar tests as the one shown in Fig. II.7.

By analyzing Figs. II.5, II.6, and II.7 it can be noted that a roughly constant strain needs to be attained so as to the steady flow is reached. It is also observed that rather long times (of until 100.000 s) are needed to reach the steady state when really low shear rates are imposed after rest. Although, by performing rate sweep tests with Carbopol dispersions in the ARES rheometer an interesting behavior is observed. More specific, if a rate sweep test with about 200 s per point starts by a very low shear rate and finishes at a high shear rate the first points plotted in the flow curve are wrong, since they were measured before the steady flow is reached. On the other hand, if a rate sweep test with about 200 s per point starts by a high shear rate and finishes at a low shear rate, the points obtained corresponding to the low shear rate range are at the values that they were expected to be, when compared to the thixotropic curves. This behavior indicates that if in one hand rather long times are needed in the low shear rate range so as to reach the steady flow from rest, on the other hand these times can be considerably shortened if the sample would have been previous sheared and no resting time was waited.

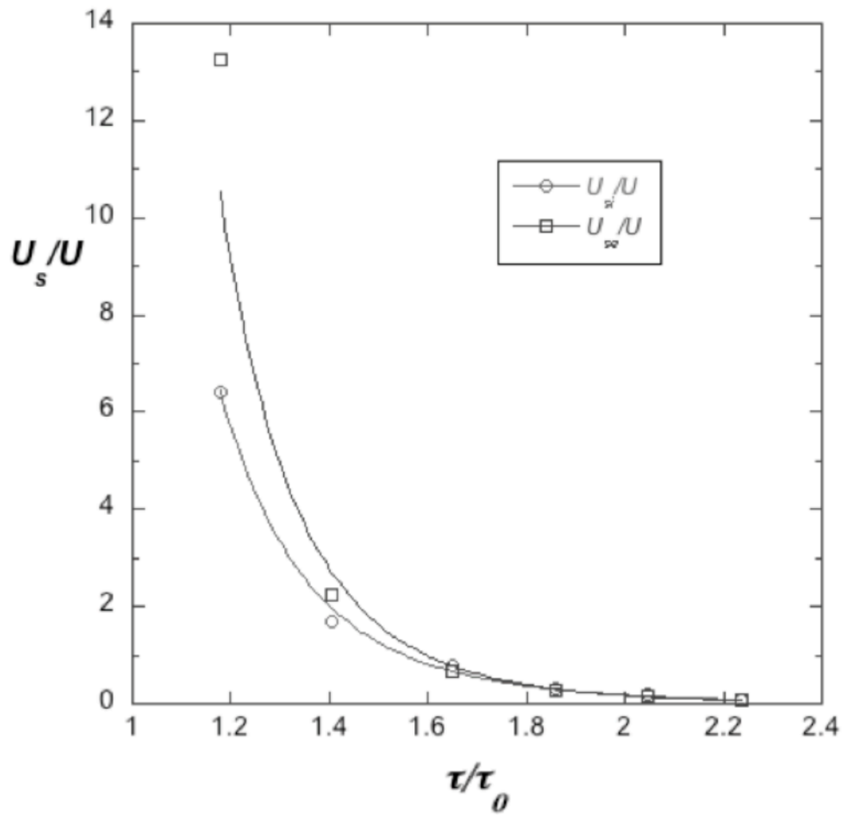

Figure II.8: Inner and outer apparent wall slip velocities.

The flow curves measured with all geometries analyzed (Fig. II.3) were used to estimate an apparent slip velocity and the results are shown in Fig. II.8. The outer wall velocity ($v_{s,\ o}$) was estimated using the grooved geometry and Eq. (2), and is given by:

$$v_{s,\ o} = (\dot{\gamma}_{va} - \dot{\gamma}_{gr})(R_o - R_i) \tag{12}$$

where $\dot{\gamma}_{va}$ and $\dot{\gamma}_{gr}$ are the shear rates measured by the rheometer, using the vane and grooved geometries respectively. This equation considers that the excess on shear rate measured with the vane geometry is due to apparent wall slip. The inner wall slip velocity was obtained using the smooth Couette geometry, assuming that the excess on shear rate values compared to the ones measured with the vane geometry is due to inner wall slip, i.e. the outer wall slip was admitted to be the same with the vane and the smooth Couette geometries. Then, the inner wall slip velocity is given by:

$$v_{s,\ i} = \left(\dot{\gamma}_{sm} - \dot{\gamma}_{gr} - \frac{v_{s,\ o}}{R_o - R_i}\right)(R_o - R_i) \tag{13}$$

With the aid of Fig. II.8, it can be noted that at lower stress, outer wall slip is higher than inner wall slip. As stresses increase, the inner and outer wall slip tend to zero.

(b) Numerical Results

Figs II.9-II.14 show the velocity and strain rate pattern for the three different geometries and two different experimental shear rate values. The dimensionless shear rate is defined using the characteristic shear rate $\dot{\gamma}_1 = (\tau_0/K)^{1/n}$. In the bob-in-cup geometry it is noted that shear rates (and shear stresses) are higher at the outer wall, as expected. The results for the vane geometry, presented in Figs. II.11 and II.12, show that a stress concentration occurs at the blades extremity. Moreover, it is observed that the material invades the space between blades, and the flow pattern deviates from that observed in the bob-in-cup geometry. As the rotation is increased, the invasion is even more critical. Figs. II.13 and II.14 show the results for the grooved geometry. It is observed that fluid invasion occurs as well but it can be pointed out that the kinematics deviation from the bob-in-cup behavior is much more critical in the vane.

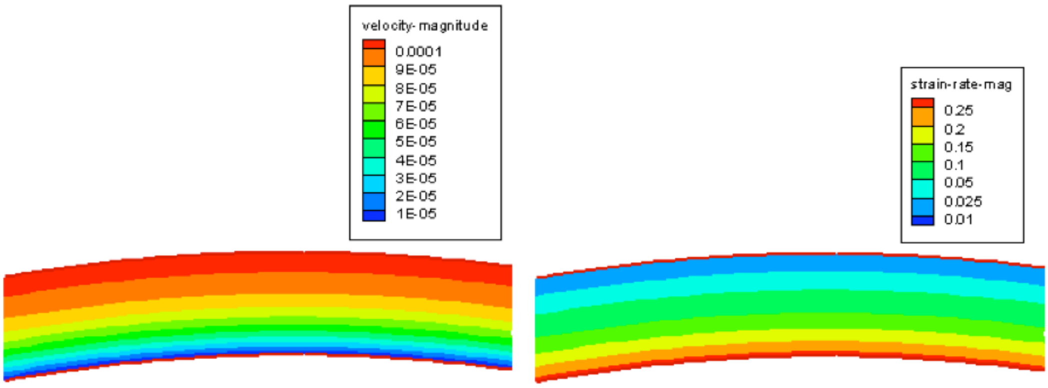

Figure II.9: Velocity and strain rate for the smooth Couette geometry, and $\dot{\gamma}_{exp}/\dot{\gamma}_1 = 4.4 \times 10^{-3}$.

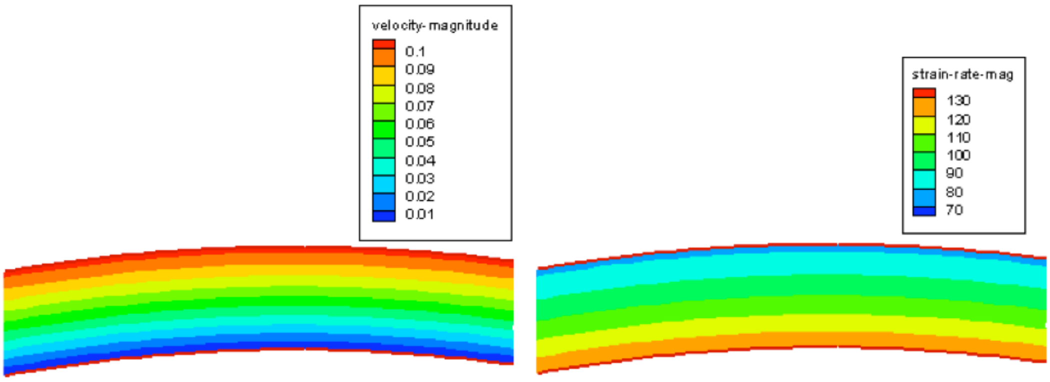

Figure II.10: Velocity and strain rate for the smooth Couette geometry, and $\dot{\gamma}_{exp}/\dot{\gamma}_1 = 4.4$.

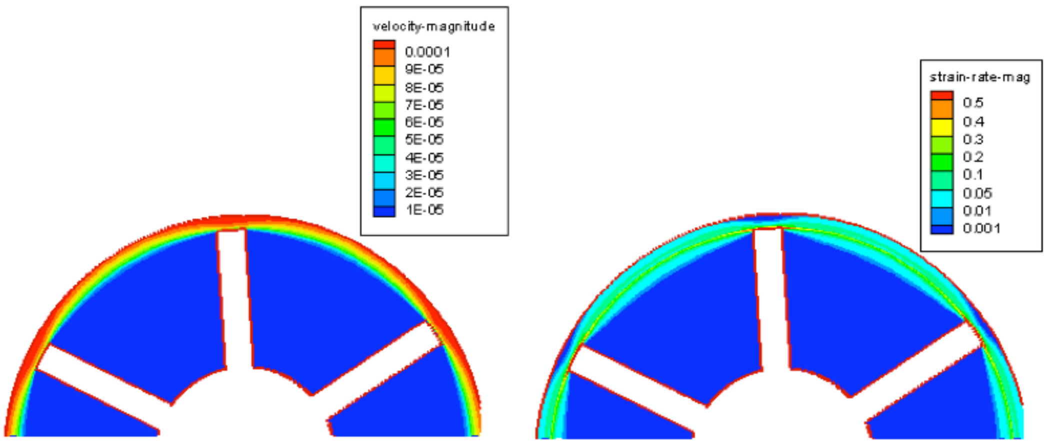

Figure II.11: Velocity and strain rate for the vane geometry, and $\dot{\gamma}_{exp}/\dot{\gamma}_1 = 4.4 \times 10^{-3}$.

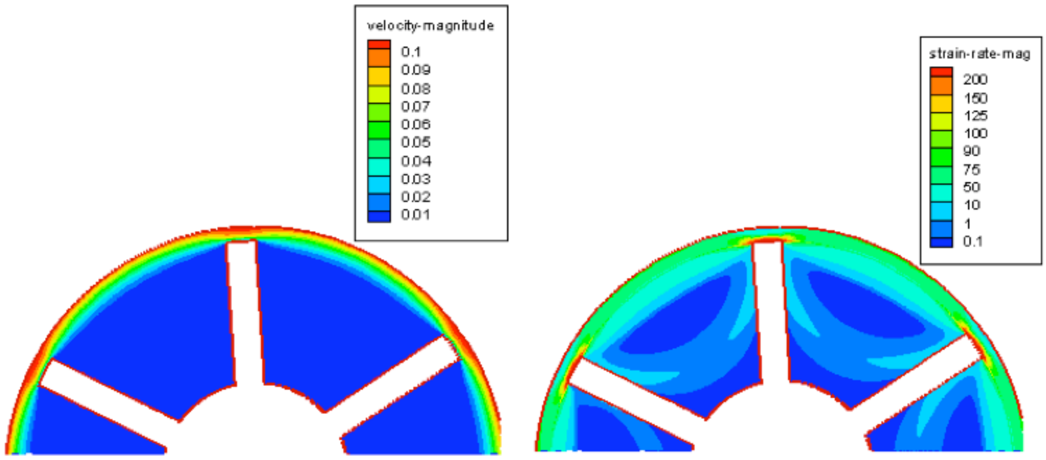

Figure II.12: Velocity and strain rate for the vane geometry, and $\dot{\gamma}_{exp}/\dot{\gamma}_1 = 4.4$.

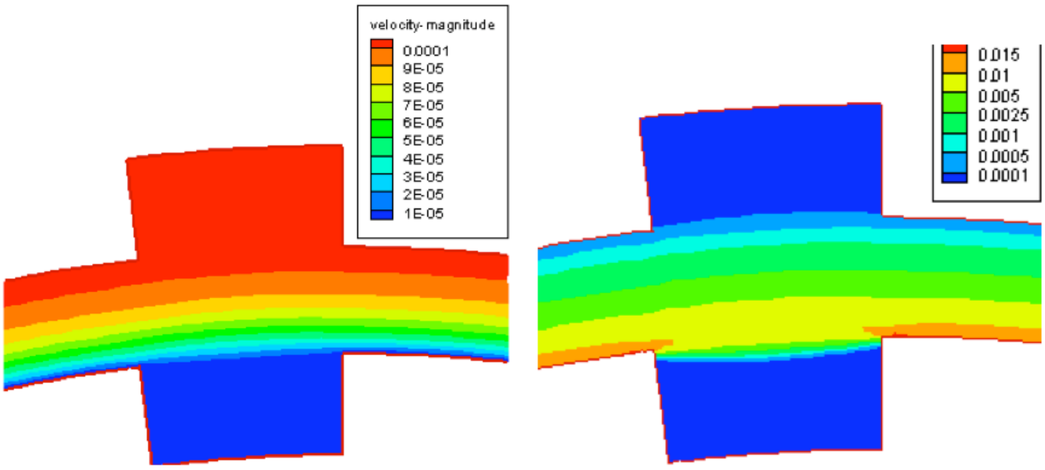

Figure II.13: Velocity and strain rate for the grooved Couette geometry, and $\dot{\gamma}_{exp}/\dot{\gamma}_1 = 4.4 \times 10^{-3}$.

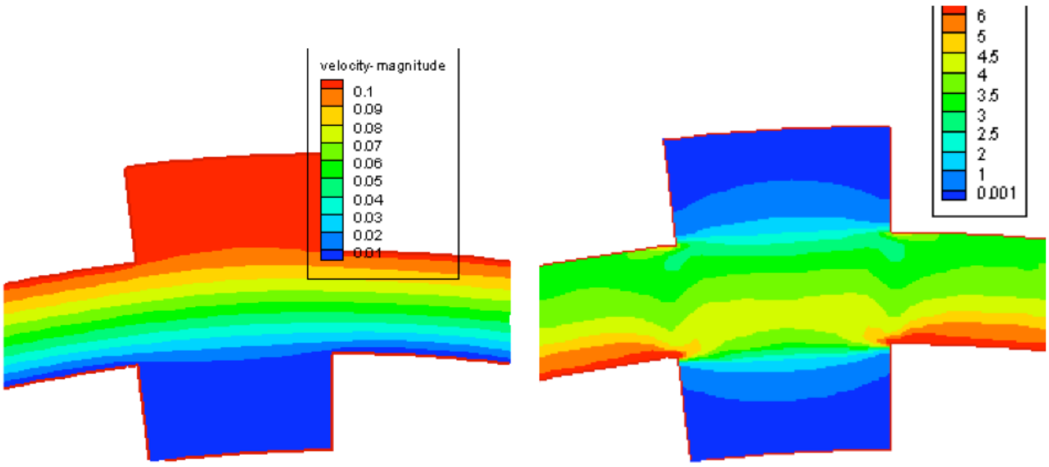

Figure II.14: Velocity and strain rate for the grooved Couette geometry, and $\dot{\gamma}_{exp}/\dot{\gamma}_1 = 4.4$.

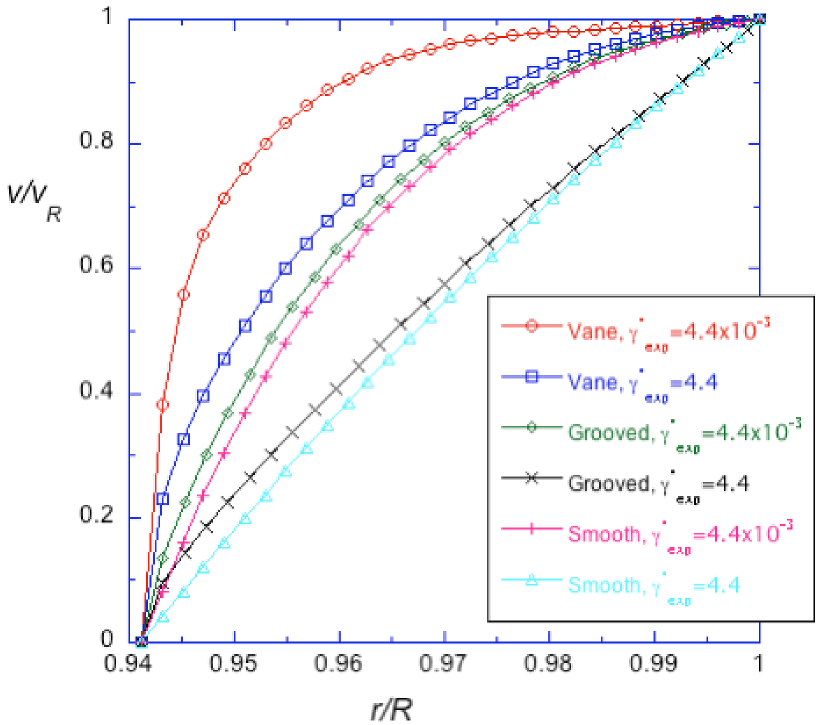

Figure II.15: Velocity profile for the three geometries and dimensionless experimental outer wall shear rate equal to 4.4×10^{-3} and 4.4.

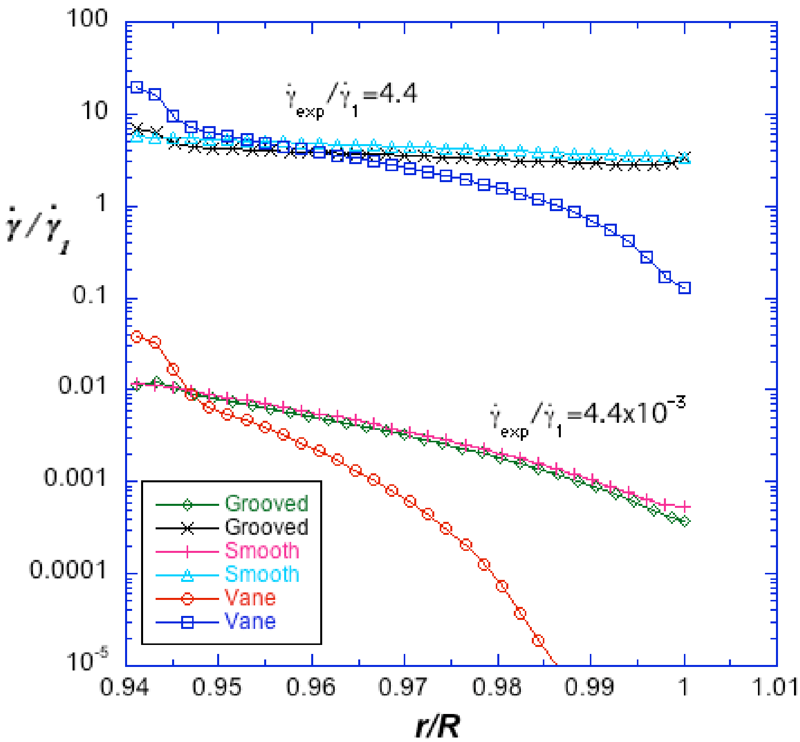

Figure II.16: Strain rate profile for the three geometries and dimensionless experimental outer wall shear rate equal to 4.4×10^{-3} and 4.4.

Figs. II.15 and II.16 show the dimensionless velocity ($v_R = \Omega R_o$) and shear rate profiles for the three geometries with outer wall dimensionless shear rate equal to 4.4×10^{-3} and 4.4. It can be observed for lower shear rates (lower rotations) that the velocity profile is highly non-linear, which could lead to errors in the experimental viscosity evaluation (see Eqs. (2) and (3)). It is also observed that the grooved and bob-in-cup profiles are similar at this range of rotation, showing that the grooved flow pattern in the annular space can be considered similar to the bob-in-cup geometry.

Fig. II.17 shows the inner and outer wall shear stress as a function of the imposed shear rate. It is noted that outer wall shear stresses are lower than the inner ones. The outer wall shear stress is equal for the vane and bob-in-cup geometries, and the grooved and vane inner wall shear stresses deviate from the bob-in-cup one, due to flow kinematics.

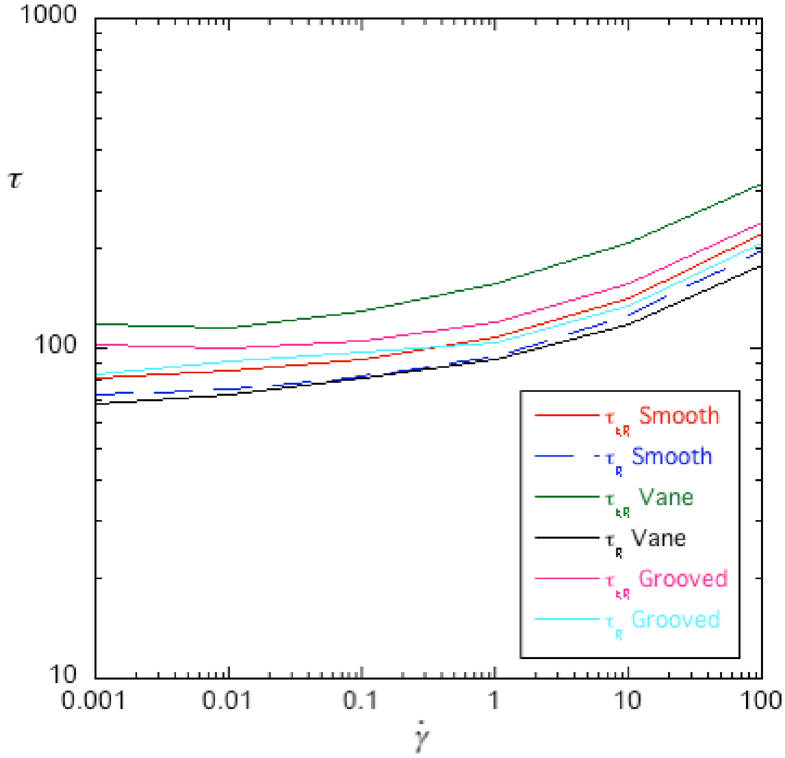

Figure II.17: Inner and outer shear stress for the three geometries.

(c) Comparison between experimental and numerical results

A comparison between numerical and experimental results is shown in Fig. II.18. It is observed that the inner wall shear stress obtained experimentally with the grooved geometry is similar to the numerical bob-in-cup geometry, showing that no slip is occuring in the experiments in this geometry.

However, both bob-in-cup and vane experimental results show that wall slip is occuring.

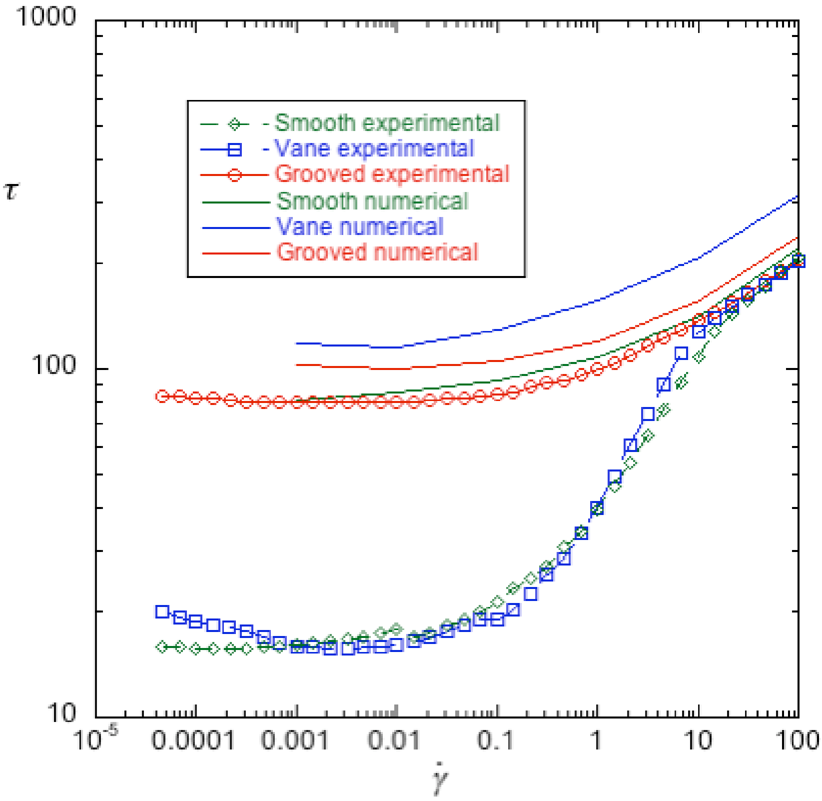

Figure II.18: Comparison of inner wall shear stress between experimental and numerical results.

II.6 Final Remarks

In this chapter, a numerical and experimental investigation was performed to analyze apparent wall slip in rheological measurements of viscoplastic materials in rotational rheometers. Three different geometries were used in the experiments: the smooth Couette, the simple vane and the grooved Couette. In addition, an analysis of rheometrical data of Carbopol dispersions was realized so as to clarify the rheological behavior of viscoplastic materials. It was shown that if in one hand rather long times are needed in the low shear rate range so as to reach the steady flow from rest, on the other hand these times can be considerably shortened if the sample would have been previous sheared and no resting time was waited. This behavior was attributed to the fact that there is a minimum strain that needs to be attained so as to the steady flow can be reached.

Numerical simulations were executed using the finite volume technique and the Fluent software. It was observed that for viscoplastic materials, apparent wall slip occurs mainly at lower shear stresses. At this range, the outer wall slip velocity is much higher than the inner one for the Carbopol dispersions studied, contradicting Buscall et al. [42] who found no slip at the outer cylinder wall for weakly attracted particle dispersions. At higher shear stresses, no slip was detected, and all geometries perform well in rheological measurements. It was also shown that flow kinematics is affected in the vane and grooved geometries, which could lead to experimental errors in viscosity measurements. At last it is important to point out that the grooved geometry performance was much better than the other ones in the rheological measurements realized, but more investigation is necessary.

II.7 Note

In this chapter it was realized an analysis of some viscometric flows involving viscoplastic materials. Sec. II.1 is a bibliography review about the subject performed by myself. In Sec. II.2 the governing equations found in the bibliography review are shown. In Sec. II.3 the experiments realized by myself with the help of Paula Mey and Cátia Lima are described. Sec. II.4 deals with the numerical solution of some viscometric flows permormed by myself in partnership with prof. Naccache. In Sec. II.5 the results obtained are shown and discussed, and in Sec. II.6 some final remarks are presented. Prof. de Souza Mendes guided us in this research.